

Article

Strain Rate Contribution due to Dynamic Recovery of Ultrafine-Grained Cu–Zr as Evidenced by Load Reductions during Quasi-Stationary Deformation at $0.5 T_m$

Wolfgang Blum ^{1,*}, Jiří Dvořák ², Petr Král ², Philip Eisenlohr ³  and Vaclav Sklenička ²

¹ Department of Materials Science, Institute I, University of Erlangen-Nuremberg, Martensstr. 5, D-91058 Erlangen, Germany

² Institute of Physics of Materials, Czech Academy of Sciences, Žitkova 22, CZ-616 62 Brno, Czech Republic; dvorak@ipm.cz (J.D.); pkral@ipm.cz (P.K.); sklen@ipm.cz (V.S.)

³ Chemical Engineering and Materials Science, Michigan State University, East Lansing, MI 48824, USA; eisenlohr@egr.msu.edu

* Correspondence: wolfgang.blum@fau.de

Received: 24 September 2019; Accepted: 21 October 2019; Published: 26 October 2019



Abstract: During quasi-stationary tensile deformation of ultrafine-grained Cu-0.2 mass%Zr at 673 K and a deformation rate of about 10^{-4} s^{-1} load changes were performed. Reductions of relative load by more than about 25% initiate anelastic back flow. Subsequently, the creep rate turns positive again and goes through a relative maximum. This is interpreted by a strain rate component $\dot{\epsilon}^-$ associated with dynamic recovery of dislocations. Back extrapolation indicates that $\dot{\epsilon}^-$ contributes the same fraction of $(20 \pm 10)\%$ to the quasi-stationary strain rate that has been reported for coarse-grained materials with high fraction of low-angle boundaries; this suggests that dynamic recovery of dislocations is generally mediated by boundaries. The influence of anelastic back flow on $\dot{\epsilon}^-$ is discussed. Comparison of $\dot{\epsilon}^-$ to the quasi-stationary rate points to enhancement of dynamic recovery by internal stresses. Subtraction of $\dot{\epsilon}^-$ from the total rate yields the rate component $\dot{\epsilon}^+$ related with generation and storage of dislocations; its activation volume is in the order expected from the classical theory of thermal glide.

Keywords: Cu–Zr; ECAP; ultrafine-grained material; deformation; dynamic recovery; transient; load change tests

1. Introduction

In materials science one is used to think in terms of strain hardening and recovery: The dislocation density increases with plastic strain so that the material hardens; recovery decreases this density with time so that the material softens. However, this view is too simple as the recovery processes get biased under stress so that dynamic recovery, i.e., recovery under stress, also causes strain. Recovery by cross slip is an early and well known example. When the rate of strain due to recovery decreases, the material may seem to harden even though it recovers. The present work deals with this surprising effect in an ultrafine-grained material with high content of high-angle boundaries (HABs).

In a companion paper the quasi-stationary (qs) deformation strength of ultrafine-grained (ufg) Cu–Zr has been described. In qs deformation storage and recovery of dislocations approximately balance each other so that the dislocation density ρ remains approximately constant, i.e.,

$$\dot{\rho}^+ \approx \dot{\rho}^- \quad (1)$$

Storage occurs after expansion of dislocation loops on slip planes (Figure 1: 'dislocations in'). Dynamic recovery is coagulation of dislocation loops after dipole capture (Figure 1: 'dislocations out'). The recovery processes may be spatially concentrated at crystallite boundaries or may be more equally distributed as in solid solutions of class I-type with solute drag on dislocations [1,2]. Recovery generally requires dislocation motion outside the primary slip plane by climb or cross slip [3].

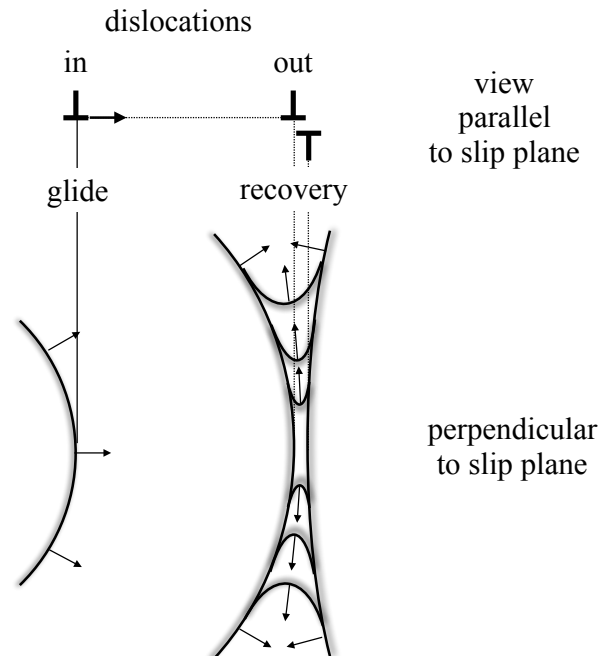


Figure 1. Scheme of dislocation glide with generation and storage of dislocations ('dislocations in') and dynamic recovery of dislocations ('dislocations out') viewed perpendicular and parallel to glide plane.

In the view in a direction parallel to the glide plane, where dislocations appear as points (Figure 1), recovery seems to make a negligible contribution to strain during annihilation of dislocation dipoles. Therefore, dynamic recovery is usually not considered as a process generating strain. Rather, the models regard strain as a result of thermally activated expansion of slipped areas bounded by dislocation lines with positive curvature that have to overcome a significant athermal stress component (forest dislocations, long-range back stresses from boundaries). In this picture the existing dislocations act as *obstacles* to dislocation glide. However, the view in a direction perpendicular to the slip plane shows that strain may well be generated during the process of coagulation of dislocation loops in recovery as negatively curved dislocation segments straighten [4,5]. Here, the interaction of dislocations *supports* the expansion of slipped areas by glide rather than opposing it. The difference in driving forces means that the kinetics of generation of dislocation length by glide of positively curved dislocations moving through the existing dislocation structure differs from that of decrease of dislocation length by motion of negatively curved dislocations. Therefore, it makes sense to treat the rate $\dot{\epsilon}_{pl}$ of plastic deformation as sum of storage strain occurring at a rate $\dot{\epsilon}^+$ and recovery-strain occurring at a rate $\dot{\epsilon}^-$ [4,5]:

$$\dot{\epsilon}_{pl} = \dot{\epsilon}^+ + \dot{\epsilon}^- \quad (2)$$

In the literature, there are a couple of examples of processes of type $\dot{\epsilon}^-$, where recovery is coupled with glide or glide is associated with recovery (class I alloys with viscously moving dislocations [1,2,6], knitting-out of dislocations from LABs [7–9], accommodation processes at HABs [10], strain coupled with migration of LABs (e.g., [11]) and HABs (e.g., [12])). Compared to $\dot{\epsilon}^+$ the recovery-strain rate $\dot{\epsilon}^-$ has received little attention (see e.g., [3,13]). In monotonic qs deformation, the two terms $\dot{\epsilon}^+$ and $\dot{\epsilon}^-$ are coupled via condition Equation 1. To investigate recovery of dislocation lines separately from storage of dislocations, one must decouple the two processes. This can be done by perturbing monotonic

flow by a sudden change of the force F at which the specimen deforms. Such a perturbation abruptly changes the forces exerted per length of dislocations and triggers reversible time-dependent dislocation motions (e.g., bowing/unbowing). The strains caused by those motions are called anelastic. So the total inelastic strain rate is

$$\dot{\epsilon}_{\text{inel}} = \dot{\epsilon}_{\text{pl}} + \dot{\epsilon}_{\text{anel}}. \quad (3)$$

Figure 2 schematically shows the response to a change from F_0 to $F_r \equiv R F_0$ at a time t_0 and an inelastic strain $\epsilon_{r,0}$. Consider relatively small changes of the relative load R (cases a and b in Figure 2). These cause relatively small changes in inelastic deformation rates from the value $\dot{\epsilon}_{r,0}$ before the R -change to a new value $\dot{\epsilon}_{r,1}$. Anelastic strains are negligible. Just after the R -change, the dislocation structure and the rest of the microstructure are virtually the same as before ('constant structure'), but the glide velocity of dislocations has changed due to the change of the stresses acting on the dislocations. The ratio $\dot{\epsilon}_{r,1}/\dot{\epsilon}_{r,0}$ is widely used to get a measure of the activation volume V^+ of thermally activated dislocation glide as described in more detail in Appendix B. A particularly large body of 'constant structure' data of $\dot{\epsilon}_{r,1}/\dot{\epsilon}_{r,0}$ has been collected for various metals and alloys by Milička in stress change tests during creep at elevated temperatures [14–16].

Now we consider relatively large F -changes (cases c and d in Figure 2). Anelastic strains are no longer negligible and diminish $\dot{\epsilon}_{\text{inel}}$ compared to $\dot{\epsilon}_{\text{pl}}$ (Equation (3)). At sufficiently low R , the forces acting on the dislocations initially get negative so that $\dot{\epsilon}_{\text{inel}}$ becomes negative directly after the R -reduction [17]. This is a consequence of internal stresses of short- and long-range nature acting on the dislocations [17] and opposing thermally activated glide of type $\dot{\epsilon}^+$. As the back flow relaxes the internal back stresses created before the R -reduction, the absolute magnitude of the rate $\dot{\epsilon}_{\text{anel}}$ declines, $\dot{\epsilon}_{\text{pl}}$ becomes dominant again, and forward deformation is reestablished at a rate $\dot{\epsilon}_{\text{pl}} = \dot{\epsilon}_{r,2}$. The preceding anelastic back flow is expected to cause only subtle changes of the dislocation arrangement and the rest of the microstructure; therefore, the rate $\dot{\epsilon}_{r,2}$, measured short after the period of back flow, has also been addressed as 'constant structure' rate. However, it is clear that this is not fully correct (see Equation (4)).

In the further course of the transient after large R -reductions, $\dot{\epsilon}_{\text{anel}}$ becomes negligible so that $\dot{\epsilon}_{\text{inel}} \approx \dot{\epsilon}_{\text{pl}}$. A remarkable result is that $\dot{\epsilon}_{\text{inel}}$ generally *decreases* for long times as schematically indicated by the dashed curve. This behavior is not well known in the community, although it is regularly found whenever investigated, independent of materials and pretreatment. It is distinct from the so-called inverse transient behavior where the decrease of $\dot{\epsilon}_{\text{inel}}$ with strain after R -reduction occurs in the whole interval $0 < R < 1$, and not only at small R . One reason for the lack of knowledge about decreasing $\dot{\epsilon}_{\text{inel}}$ after large R -reductions is, that long-term tests are required for such observations, covering test times distinctly beyond the extended period of back flow. Such tests have been done by Blum and coworkers on a number of materials including e.g., Al-5Mg (class I alloy) [18,19], Al-Zn (class II alloy) [20], and pure LiF [21] and by Van Swygenhoven and coworkers on nanocrystalline Ni and Ni-Fe [10,22,23]. In these tests direct evidence for ongoing net recovery of dislocations was obtained. A natural explanation of the decrease of $\dot{\epsilon}_{\text{inel}}$ after perturbation of plastic flow by a large R -reduction is that the recovery rate component $\dot{\epsilon}^-$ decreases, because the driving force for recovery declines during the decrease of ρ and other crystal defects to the lower level in the new qs state at the lower stress.

The same process of net recovery must also be expected when a deformed specimen is simply unloaded to $R = 0$ and subsequently annealed at elevated temperature higher than the deformation temperature. This type of experiment has been done by Hasegawa, Yakou and Kocks on pure Al [24,25] that was deformed at ambient temperature and then quickly heated to elevated temperature. The result was qualitatively the same as the result of unloading at fixed temperature described before: net *back* flow due to anelastic strains was followed by net *forward* flow at declining rate. This forward flow at zero stress after predeformation was interpreted by the authors as consequence of recovery; the recovery was suggested to result from reaction of neighboring polarized dislocation walls.

So far, comprehensive studies of the transient response to stress reductions are missing in the case of ECAP-processed ufg materials. Two tests performed on ufg Cu [26] showed a decrease of creep rate

after relative stress reductions to $R = 0.77$ and 0.70 that could be explained in terms of decreasing recovery–strain rate. The present study of transient deformation after qs deformation of ufg Cu–Zr has these main objectives:

- demonstrate that the transient response to load changes can be studied in standard tensile creep machines with load control,
- advertise a new type of plot [27] (Figure 3e) displaying the full strain-time evolutions of all tests of a series with different degrees of unloading at reasonable resolution,
- show that the transient behavior of an ufg material is qualitatively the same as that of cg materials, including an initial period of strain mainly due to recovery,
- discuss the mechanism of dynamic recovery in qs and transient deformation with special regard to the influence of internal stresses.

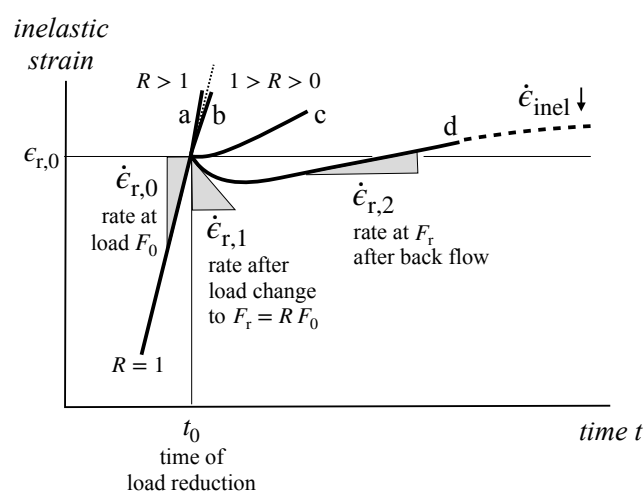


Figure 2. Response of inelastic strain to fast changes of creep load from F_0 to $F_r = RF_0$ during deformation at time t_0 and strain $\epsilon_{r,0}$ for (a) small R -increase, (b) small R -decrease, (c) medium R -decrease causing $\dot{\epsilon}_{r,1} = 0$, (d) large R -decrease causing net back flow.

2. Experimental Details

As described in more detail in the companion paper [28], our particle-stabilized material, called p Cu–Zr, was produced by severe predeformation at ambient temperature in p passes of equal channel angular pressing (ECAP) on route B_C . Its material parameters are approximated by those of pure Cu provided in the data compilation of Frost and Ashby [29]: Burgers vector $b = 2.56 \times 10^{-10}$ m, elastic shear modulus $G = 3.58 \times 10^4$ MPa, melting point $T_m = 1356$ K. The test temperature was $T = 673$ K = $0.5 T_m$.

Deformation was started by applying tensile loads F to flat specimens with initial values of gauge length $l_0 = 10$ mm and cross section S_0 of usually ≈ 12 mm². The standard creep machines used in this work were designed for long-term measurements of creep strain accumulation at *constant* load, not for precisely following small strain changes after load changes. The reproducibility of measurements of back flow was worse than in Milička’s tests [14–16], but better than originally expected, although some artifacts from unmotivated jumps in the extensometer system or errors in σ_{eng} occasionally seem to have occurred (see e.g., the black curve in Figure 3b after unloading). In the periods of deformation (creep) at constant load the inelastic strain rate is practically identical to the measured total strain rate $\dot{\epsilon}_{tot}$ as the elastic strain rate $\dot{\epsilon}_{el}$ is negligible. In the periods of fast changes of load F this is no longer so. Appendix A explains the procedure taken to get the inelastic strain ϵ_{inel} at acceptable accuracy. The inelastic strain rate follows from ϵ_{inel} as $\dot{\epsilon}_{inel} = \Delta\epsilon_{inel}/\Delta t$ where $\Delta\epsilon_{inel}$ must be chosen larger than the experimental noise. This was achieved by data smoothing with the open software SmooMuDS [30].

3. Results

3.1. Transients as Function of Time

A change of load from a start value F_0 corresponding to an engineering stress $\sigma_{\text{eng}} = F_0/S_0$ to a new value $F = R F_0$ at time t_0 and inelastic strain ϵ_0 initiates a transient response. To display all transients of largely different durations in the same plot, a logarithmic time scale is used in Figure 3; the constants 10 s in the time-scale and 0.01 in the ϵ_{inel} -scale serve to bring the start of transient into the field of view. Figure 3a–c shows three tests with relative load reductions to by 60% to $R = 0.4$. The reductions deliberately were performed in steps to explore the behavior at intermediate stresses (Figure 3a). The strain evolution varies with step height and step length. In some cases net forward deformation continued during the first unloading steps (Figure 3b). However, the strains accumulated there were small and no significant effect on the values of $\dot{\epsilon}_{\text{inel}} > 0$ after the reductions was observed. This is different in the periods of back flow ($\dot{\epsilon}_{\text{inel}} < 0$). Such a difference must be expected because back flow relaxes the internal stresses driving it. However, our work does not focus on back the flow triggered by the perturbation by R -reductions, but on the subsequent forward flow (see Figure 3b). Figure 3c displays the *forward* strain rates $\dot{\epsilon}_{\text{inel}} > 0$ after R -reduction that reappear after about 20 to 30 ks when back flow has faded, $\dot{\epsilon}_{\text{anel}}$ has become negligible and $\dot{\epsilon}_{\text{inel}} \approx \dot{\epsilon}_{\text{pl}}$. In the beginning, the uncertainty in $\dot{\epsilon}_{\text{inel}}$ is large, because relatively small strain intervals $\Delta\epsilon_{\text{inel}}$ were used in determination of $\dot{\epsilon}_{\text{inel}}$ (compare Equation (2)).

Two of the $\dot{\epsilon}_{\text{inel}}$ -curves in Figure 3c still appear somewhat noisy. Yet further smoothing of data was avoided because the $\dot{\epsilon}_{\text{inel}}$ -variations seem to have a real origin in slow T -fluctuations caused by the control system. The two gray curves for 8Cu–Zr in subfigure b show the measured $\dot{\epsilon}_{\text{inel}}$ -extremes. They differ by a factor of 3 to 4 in $\dot{\epsilon}_{\text{inel}}$. We ascribe that to the aforementioned inhomogeneity of the grain structure of 8Cu–Zr. The upper gray curve for 8Cu–Zr is quite similar to the black curve for 12Cu–Zr. We conclude from this result that, apart from the scatter of the initial microstructure produced by the thermomechanical history, there is no significant difference between the ufg materials 8Cu–Zr and 12Cu–Zr.

Figure 3d–f gives the overview of all R -reduction tests performed in this work. Again, we focus on the forward flow observed *after* the anelastic back flow. The curves in Figure 3f derived from Figure 3e are arranged in a fairly consistent sequence corresponding to the loads shown in Figure 3d. This underscores the quality of the length measurements in our creep machines although these were not built for load change tests. For $R \leq 0.3$ a transient decrease of the (forward) strain rate $\dot{\epsilon}_{\text{inel}} > 0$ is evident.

Figure 4 shows the times t_{back} (circles) for anelastic back flow taken from the length-time recordings. Due to differences in unloading histories and uncertainties in length measurement the scatter is large. The dashed line corresponds to the dashed curve from Figure 3f approximating the boundary of back flow. For $R > 0.75$ the time interval of back flow is immeasurably small. So back flow becomes negligible here and deformation goes on at positive rate directly after the load reduction.

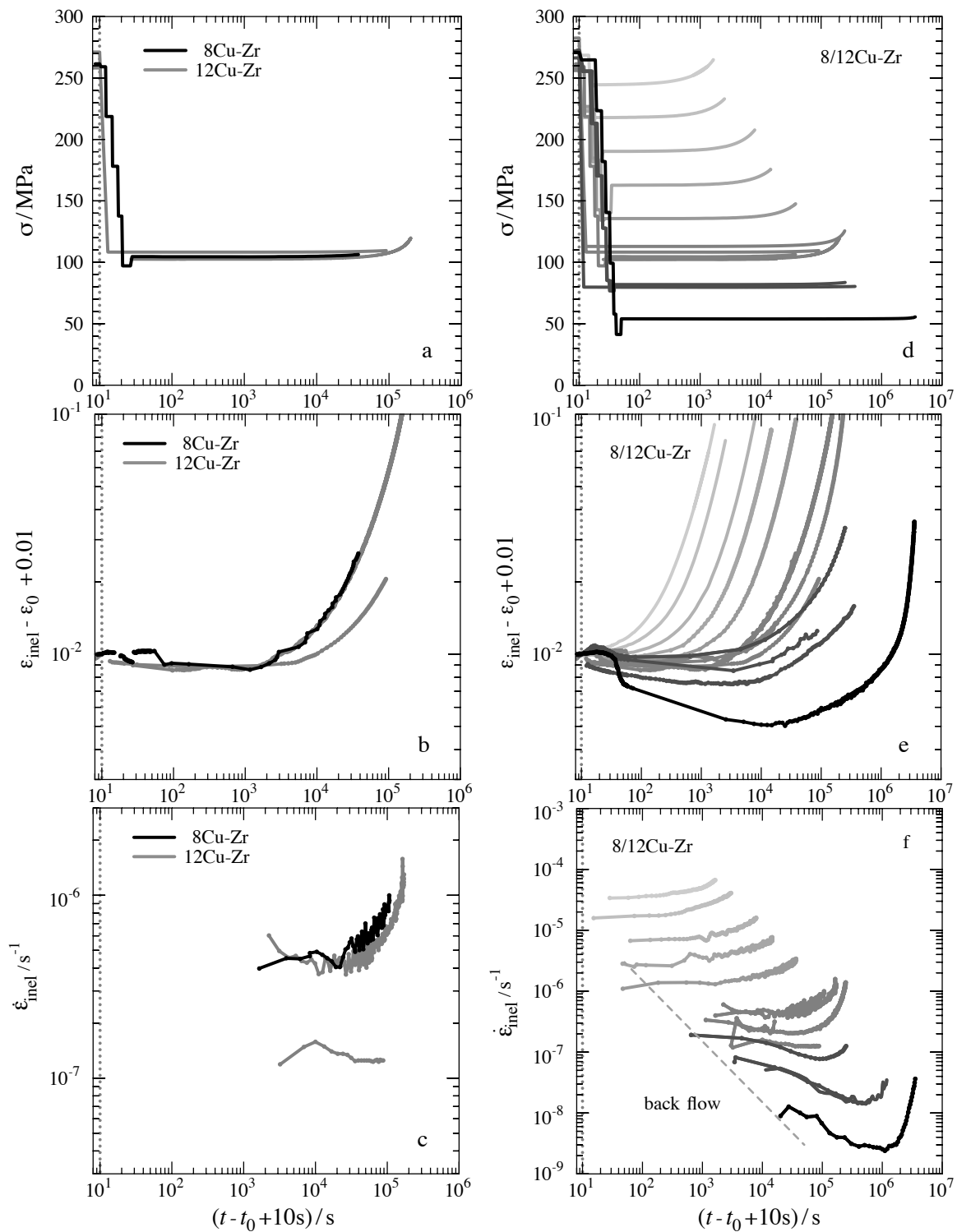


Figure 3. (a) Stress σ , (b) strain ϵ_{inel} , and (c) strain rate $\dot{\epsilon}_{inel}$ as function of time t in tests for 8Cu-Zr and 12Cu-Zr with stepwise load reduction to (a–c) $R = 0.4$ and (d–f) all R ; dashed line in (f) approximates boundary of back flow.

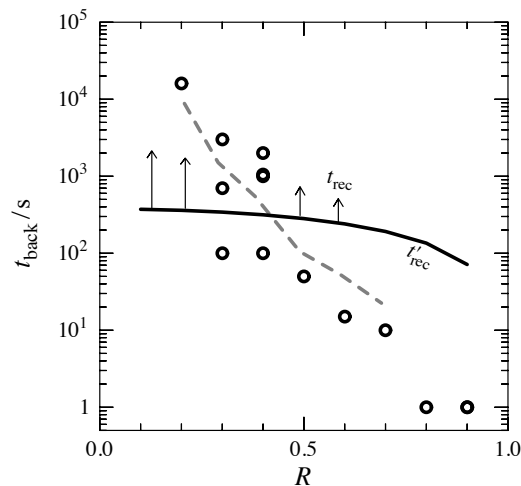


Figure 4. Times t_{back} for anelastic back flow (circles, from Figure 3e) compared to lower bound t'_{rec} of times t_{rec} for dynamic recovery toward the new qs state as function of R for $\sigma_{r,0} = 275$ MPa; dashed line corresponds to dashed line in Figure 3f.

3.2. Transients as Function of Strain

Dislocation generation needs strain. Therefore, the strain ϵ_{inel} is much more closely related to the microstructural evolution than the testing time t . So the evolution of deformation strength ($\sigma, \dot{\epsilon}_{\text{inel}}$) is commonly displayed on a strain scale. Figure 5 exhibits the transients of Figure 3f as function of ϵ_{inel} . As σ increases at constant load F , $\dot{\epsilon}_{\text{inel}}$ increases even if the microstructure is constant. This effect was eliminated by correcting $\dot{\epsilon}_{\text{inel}}$ (see caption). The corrected curves in Figure 5 should be horizontal in the qs state if the grain and phase structure remains constant. This is indeed found for large R near 1. For smaller R the curves exhibit a positive slope in the whole strain interval. This means that slow microstructural changes are going on throughout the test. Comparison of the dotted and the solid curves at $R = 0.4$ and 0.3 shows that these changes are the same in tests with and without R -reduction. At the lowest R of 0.2 (80% unloading) deformation is slowest and the structural changes including dislocations are largest. Consequently, softening is most pronounced here. The curve for $R = 0.2$ was followed for 42 days before it was interrupted without any indications of fracture; note that the $\dot{\epsilon}(\epsilon)$ curve is concave, not convex as in fracture. In [28] the softening has been shown to be a consequence of microstructural coarsening, in particular grain coarsening. This means that only the short-term portions of the curves after R -reduction show the transient response to perturbation of the dynamic equilibrium of storage and recovery of dislocations in the qs state at t_0 .

Note that the character of this short-term portion of the transients changes significantly with R . For small R -reductions to $R \geq 0.5$ there is a relative *increase* of $\dot{\epsilon}_{\text{inel}}$ compared to the qs curve at reduced R . This is known as normal transient behavior: the material softens due to coarsening of the cellular dislocation structure towards the new dynamic equilibrium state. However, for large R -reductions to $R < 0.5$ and $\dot{\epsilon}_{\text{inel}} \leq 10^{-7} \text{ s}^{-1}$ there is an initial *decrease* of $\dot{\epsilon}_{\text{inel}}$.

Figure 6 displays the constant structure rates $\dot{\epsilon}_{r,1}$ and $\dot{\epsilon}_{r,2}$ that were measured at the beginning of the transients and after anelastic back flow, respectively (see Figure 2). Figure 6a shows that $\dot{\epsilon}_{r,1}$ falls to zero near $R = 0.76$ and becomes negative (back flow) for lower R . Following Milicka [14], the data were approximated by a sinh-expression

$$\dot{\epsilon}_{r,1} = k_1 \sinh(V(\sigma - \sigma_i)/(M k_B T)) \quad k_1 = 0.0885, \sigma_i = 0.76 \sigma_{r,0}, \quad (4)$$

giving the solid grey line with change from positive to negative (back flow) rates $\dot{\epsilon}_{r,1}$. Figure 6b shows the positive rates $\dot{\epsilon}_{r,2}$ after back flow.

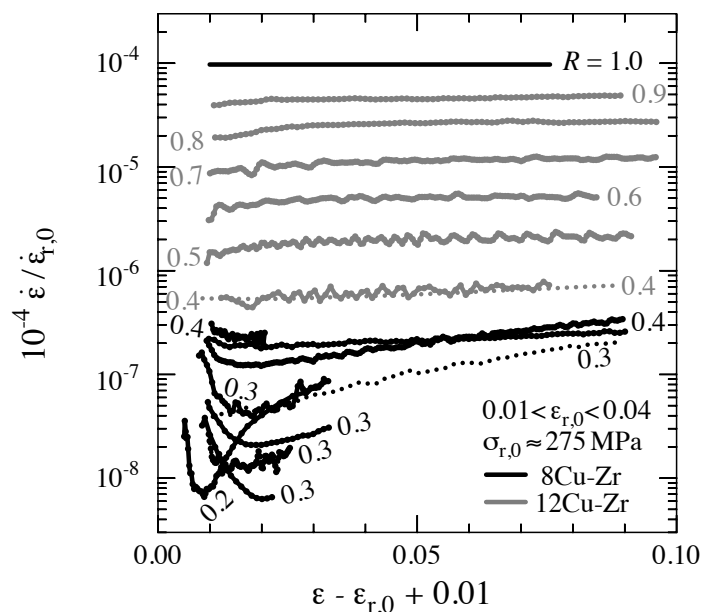


Figure 5. Normalized strain rate as a function of normalized strain after load reduction from $\sigma_{eng} = 250$ MPa to a relative load R for 12Cu–Zr (grey lines) and 8Cu–Zr (black lines); the increase of $q_s \dot{\epsilon} \propto \sigma^{n_{qs}}$ was eliminated with $n_{qs} = 6$ from [28].

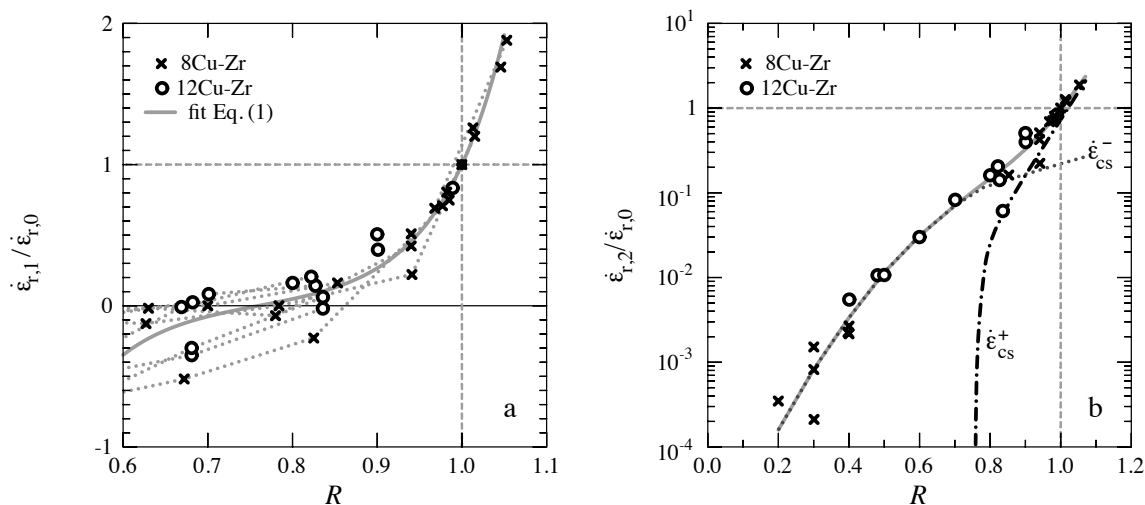


Figure 6. Normalized constant structure strain rate $\dot{\epsilon}_r$ after qs deformation of 8/12Cu–Zr at $\sigma_{r,0} \approx 275$ MPa as function of relative creep load R : (a) $\dot{\epsilon}_{r,1}$, grey dotted lines connect data from same test with stepwise load reduction, (b) $\dot{\epsilon}_{r,2}$ (symbols connected by solid grey line); on log scale with estimates of $\dot{\epsilon}_{cs}^-$ (dotted black) and $\dot{\epsilon}_{cs}^+$ (dash-dotted black); see text.

4. Discussion

Our results for ufg Cu–Zr are qualitatively quite similar to the general behavior observed for crystalline materials after a perturbation of monotonic plastic flow by load changes. For small R -reductions deformation goes on at reduced rate in forward direction according to the applied stress and the material softens with strain in parallel to the recovery of the dislocation structure. For large R -reductions deformation first goes backward before it returns to positive direction again and then continues at decreasing rate. As mentioned in Equation (1), this rate decrease parallels that of recovery and therefore may be directly linked to dynamic recovery. This can be understood from the

view that the strain rate term $\dot{\epsilon}^+$ leading to storage of dislocations disappears for small R so that the strain rate term $\dot{\epsilon}^-$ related with dynamic recovery dominates. These transient phenomena disappear while the new qs state corresponding to R is approached.

The two terms $\dot{\epsilon}^+$ and $\dot{\epsilon}^-$, corresponding to the cases 'dislocations in' and 'dislocations out' of Figure 1, have different kinetics. This difference should become apparent in those ranges of R where either $\dot{\epsilon}^+$ or $\dot{\epsilon}^-$ dominate. This is in line with the different R -dependences of the lines for $\dot{\epsilon}^+$ and $\dot{\epsilon}^-$ in Figure 6b. Milička [14–16] restricted his measurements to the R -range with $\dot{\epsilon}_{r,1} \geq 0$. In spite of this restriction, he discovered that a single mechanism of deformation obeying Equation (4) is not sufficient to describe the variation of $\dot{\epsilon}_{r,1}$ with R . So he proposed to express $\dot{\epsilon}_{r,1}$ as a sum of two terms [15,16]. This parallels the separation of $\dot{\epsilon}_{pl}$ into $\dot{\epsilon}^+$ and $\dot{\epsilon}^-$ in Equation (2).

4.1. Strain Related with Storage of Defects

From the preceding discussion we surmise that for $R \leq 0.7$ the rate $\dot{\epsilon}_{r,2}$ approximately equals $\dot{\epsilon}^-$. Extrapolating the $\dot{\epsilon}_{r,2}$ -curve for $R < 0.7$ in Figure 6 yields $\dot{\epsilon}_{qs}^-$ -values at $R = 1$ in the range of 10% and 30% of $\dot{\epsilon}_{r,0}$. In other words: the recovery–strain rate $\dot{\epsilon}_{qs}^-$ contributes about $(20 \pm 10)\%$ to the qs strain rate. $\dot{\epsilon}_{cs}^+$ follows as the difference of $\dot{\epsilon}_r$ and $\dot{\epsilon}_{cs}^-$ (Equation (2)). The stress exponent of this curve at $R = 1$ is $n_{cs}^+ = 17$ at $R = 1$. This is close to the estimate 21 derived from the theory of thermally activated glide (Equation A15). In view of the simplifications and assumptions involved, we conclude from this result that an interpretation of $\dot{\epsilon}_{cs}^+$ in terms of the classical theory of thermally activated glide over fixed repulsive obstacles in pure materials (e.g., forest dislocations) may be possible.

4.2. Strain Related with Recovery of Defects

We now turn attention to the recovery–strain rate $\dot{\epsilon}^-$. Figure 7a compares the recovery–strain rates $\dot{\epsilon}_{cs}^-$ at (approximately) constant structure from Figure 6b (dotted line) to the recovery–strain rate $\dot{\epsilon}_{qs}^-$ at qs structure (solid line) as function of stress σ . The latter is obtained from the qs strain rates $\dot{\epsilon}_{qs} \propto \sigma^6$ reported in the companion paper [28] under the assumption that the fraction $\dot{\epsilon}_{cs}^-/\dot{\epsilon}_{qs}$ in qs deformation equals ≈ 0.2 independent of stress. $\dot{\epsilon}_{cs}^-$ is larger than $\dot{\epsilon}_{qs}^-$. This can be qualitatively explained by the higher defect density and higher local stresses in the cs states inherited from the preceding deformation at the high stress $\sigma_{r,0} \approx 275$ MPa compared to the qs states established at lower stresses $\sigma < \sigma_{r,0}$. So far there is no accepted detailed model of dynamic recovery and its strain rate contribution $\dot{\epsilon}^-$. Strain contributions from recovery of individual dislocations stored at recovery sites, probably internal crystal boundaries (LABs, HABs), and from recovery of boundaries by migration need to be considered.

One may ask to which extent the recovery–strain rate gets reduced in the period of back flow before $\dot{\epsilon}_{r,2}$ is measured. It is clear that anelastic back flow relaxes internal stresses. Also, some fast recovery processes of the kind shown in Figure 1 will happen already during the period of net back flow and thereby reduce the density of recovery sites. This indicates that use of the term 'constant structure' for $\dot{\epsilon}_{cs}^-$ becomes increasingly problematic with declining R with regard to the dislocation structure and raises the question whether the constant structure assumption is wrong and anelastic back flow may even be lasting long enough to modify not only the internal stresses, but also allow the dislocation structure to evolve close to the new qs state at reduced stress. In this case $\dot{\epsilon}_{r,2}$ should become equal to the qs rate $\dot{\epsilon}_{qs}$ for low R and correspondingly low stresses. And this is in fact observed around 100 MPa, as Figure 7a shows. To answer the question we estimate a lower limit t'_{rec} of the time t_{rec} for full recovery into the new qs state. The estimate is based on the assumptions that (i) no dislocation generation takes place during the anelastic back flow even though the new qs state is based on dynamic equilibrium of generation and recovery and (ii) the maximal rate of dislocation recovery pertains throughout the back flow period even though the driving force for recovery must decrease. In the literature there is very little direct information on the evolution of the density ρ of dislocations during dynamic recovery. The reasons are that dynamic recovery is generally accompanied by dislocation glide of type $\dot{\epsilon}^+$ and that reliable observations can only be made if the dislocations can safely be

pinned up to microscopic observation. A set of data was measured in [20] for the alloy Al–Zn where pinning is possible by precipitation of particles. The data were obtained in the qs state characterized by Equation (1). It was found that the measured dislocations recovery rates $\approx \dot{\rho}^-$ were in accord with Equation (1) when the dislocation generation rate is expressed as

$$\dot{\rho}^- \approx \dot{\rho}^+ = \frac{M f_{\Lambda}}{b} \frac{\dot{\epsilon}^+}{\Lambda}. \quad (5)$$

where Λ is proportional to the mean free path of dislocations and f_{Λ} is a numerical factor near 1. For a rough estimate we set $\Lambda = d_0$, $\dot{\epsilon}_{r,0} = 10^{-4} \text{ s}^{-1}$, $f_{\Lambda} = 1$. This yields the rate $\dot{\rho}_0^-$ of dynamic dislocation recovery just before the R -reduction as $2 \times 10^{-12} \text{ m}^2 \text{ s}^{-1}$. The initial qs dislocation spacing is estimated as $\rho_{\text{qs}} = (b G / \sigma_{r,0})^2$ at $\sigma_{r,0} = 275 \text{ MPa}$. The solid line in Figure 4 shows the result for t'_{rec} . The data symbols represent the experimental data for the time period t_{back} where anelastic back flow occurs or cannot be excluded due to experimental inaccuracy. The result of this estimate is that in a large R -range the time period t_{back} available for recovery during back flow is smaller than the lower bound t'_{rec} of the time period t_{rec} of recovery needed to reach the new qs state of dislocation density. This corresponds to the observation made in situ on nanocrystalline Ni that recovery of X-line widths continues after the period of back flow [22]. So we conclude that $\dot{\epsilon}_{\text{cs}}^-$ in Figure 6b mainly represents the recovery–strain rate due to $\dot{\rho}^-$, and not the qs strain rate resulting from $\dot{\rho}^+ - \dot{\rho}^-$ -balance (Equation (1)).

The results of the present work do not allow us to deduce details about the mechanism of recovery–strain. Cross slip [31] and climb [32] are generally being considered as rate-controlling mechanisms (compare [3]). Stress concentrations at boundaries by long-range internal stresses have been used in descriptions of kinetics with the composite model [33]. LABs in coarse-grained materials [11,21] and of HABs in nanocrystalline materials [34] are being discussed as sinks of dislocations as well as of boundaries themselves (via recombination during migration). Measurements on single-crystalline LiF have led to the conclusion that migration of LABs is responsible for most or even all of the observed recovery strain [21]. (A different situation is encountered in class II alloys like Al–Mg with viscous dislocation glide due to strong solute drag and spatially homogeneous distribution of recovery events [2,18,19,35]; here long-range stresses seem to play only little role.) The insensitivity of the relative recovery–strain contribution of recovery in the qs state to the boundary misorientation is intriguing. The observation that LABs are the major carriers of recovery strain in coarse-grained (cg) materials means that generation of recovery–strain by annihilation of single dislocations (Figure 1) cannot be used to explain the recovery strain in both LAB- and HAB-dominated structures. A boundary-mediated recovery mechanism, however, may be valid in both cases. It could mean that the rates of dynamic recovery vary with the HAB-content, but the basic mechanism involving free dislocations and boundaries is the same.

Better understanding of recovery–strain may be of profound value in technical application of strong materials under conditions of varying stress σ , e.g., in stress relaxation and cyclic deformation. The period of dominant recovery–strain rate $\dot{\epsilon}^-$ after load reductions gives the unique chance to investigate the kinetics of dynamic recovery alone without influence of the storage strain rate $\dot{\epsilon}^+$. One option is to perform *secondary* load change tests in this period after a primary large load reduction. Such secondary load changes have been started on Al [36] and recently continued on nc Ni [22,23]. The stress sensitivity in the period of $\dot{\epsilon}_{\text{qs}}^-$ -dominance was found to be much smaller than the qs stress sensitivity n_{qs} . Another option is to develop a *model* of dynamic recovery describing both the stress dependences of $\dot{\epsilon}_{\text{cs}}^-(R)$ at constant structure and of $\dot{\epsilon}_{\text{qs}}^-$ in the qs state.

An obvious question to be answered by a model is why the recovery–strain rate $\dot{\epsilon}_{\text{cs}}^-$ at constant structure is so similar to the qs strain rate $\dot{\epsilon}_{\text{qs}}$ (Figure 7a). At least part of the answer seems to lie in internal stresses [37]. It is probable that recovery processes are concentrated at relatively hard regions, in particular crystallite boundaries, where the local stress σ_{h} is enhanced relative to the applied stress

by a local forward stress σ_f . In the following we apply the phenomenological approach used in [37] to the present case. Assume that $\dot{\epsilon}^-$ varies with a power q of σ_h :

$$\dot{\epsilon}_{cs}^- = f_0^- \dot{\epsilon}_{r,0} \left(\frac{\sigma_h}{\sigma_{h,0}} \right)^q; \tag{6}$$

f_0^- connects $\dot{\epsilon}_{cs}^-$ to the strain rate $\dot{\epsilon}_{r,0}$ before the stress reduction; σ_h is the sum of applied stress $R\sigma_{r,0}$ after R -reduction and local internal forward stress $\sigma_f = f_{rel}\sigma_{f,0}$, i.e., $\sigma_h = R\sigma_{r,0} + f_{rel}\sigma_{f,0}$; here $\sigma_{f,0}$ is the forward stress at $R = 1$ before the load reduction and f_{rel} describes the relaxation of the internal forward stress during anelastic back flow before $\dot{\epsilon}_{cs}^-$ is measured; $\sigma_{h,0}$ is the starting value of σ_h at $R = 1$ and $f_{rel} = 1$ before the R -change. To give an example, f_0^- is set to 0.22, the exponent in Equation (6) is chosen as $q = 7$, and $\sigma_{f,0}$ is assumed to be $1.5\sigma_{r,0}$. With these choices Figure 7a shows $\dot{\epsilon}_{cs}^-$ as function of R for two cases. The first case $f_{rel} = 1$, i.e. no relaxation of internal forward stress during anelastic back flow, yields $\dot{\epsilon}_{cs}^-$ -values lying distinctly higher than the measured ones, but is unrealistic. In the second case f_{rel} is assumed to decrease with decreasing R as shown in Figure 7b. The thick dotted curve in Figure 7a represents the result for $\dot{\epsilon}_{cs}^-$. It was made to perfectly match the measured $\dot{\epsilon}_{cs}^-$ -curve from Figure 6b. For comparison, the line for $\dot{\epsilon}_{qs}^-$ shows the recovery-strain rate expected in the qs state, if the ratio f_0^- is independent of stress as suggested by numerous results obtained for cg materials. It is seen that although the relaxation of the internal stresses during back flow may be significant, it always keeps the recovery-strain rate generated from the dense defect structure at high stress $\sigma_{r,0}$ above the qs strain rate expected at the lower stresses acting at $R < 1$ where the qs defect density is much lower. That makes sense. The preceding exercise shows that the measured constant structure recovery-strain rates can be understood on the basis of internal forward stresses of some kind acting at the recovery sites. It must, however, naturally be expected that the decrease of the volume density of recovery sites during back flow also contributes to the decline of $\dot{\epsilon}_{cs}^-$, qualitatively marked by the downward pointing arrows in Figure 7.

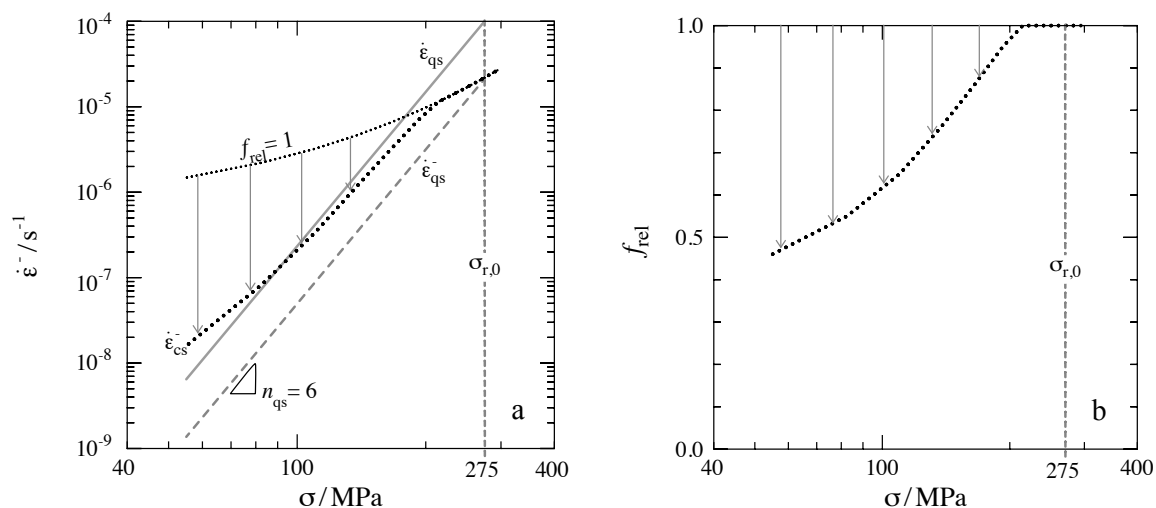


Figure 7. (a) Recovery-strain rate $\dot{\epsilon}_{cs}^-$ at constant structure after R -change from Figure 6b (black dotted) compared to qs strain rate $\dot{\epsilon}_{qs}$ (grey solid) and recovery-strain rate $\dot{\epsilon}_{qs}^-$ in the qs state (grey dashed), (b) anelastic relaxation factor f_{rel} as function of $\sigma \approx R\sigma_{r,0}$ required to model $\dot{\epsilon}_{cs}^-$ from (a) with Equation (6).

4.3. Comparison of Stress Dependences of $\dot{\epsilon}^+$ and $\dot{\epsilon}^-$ at Constant Structure

One problem with measuring the recovery-strain rate $\dot{\epsilon}^-$ is that its separation from $\dot{\epsilon}^+$ in load/stress change tests is not trivial and sometimes impossible. The separation is easy and accurate if the inflection point in the semilogarithmic $\dot{\epsilon}_{r,2}$ -curve (Figure 6b) is well pronounced. This depends

strongly on the slope of this curve at $R = 1$. This slope is mostly given by the stress exponent n_{cs}^+ of $\dot{\epsilon}^+$ (see Equation A15), i.e., the rate associated with generation of defects leading to work hardening. According to the estimate of Equation A14 n_{cs}^+ decreases inversely proportional to the temperature T .

On the other hand, the slope of the $\dot{\epsilon}^-$ -curve due to recovery is rather insensitive to T . Therefore, the separation of $\dot{\epsilon}^-$ becomes increasingly problematic when T increases. Solid solution strengthening leads to further reduction of n_{cs}^+ and the inflection point in the semilogarithmic $\dot{\epsilon}_{r,2}$ -curve (Figure 6b) may disappear completely (e.g., in Al–5Mg [14,19] and Fe–Si [15]). Then the separation of $\dot{\epsilon}^+$ and $\dot{\epsilon}^-$ may be based on the fact that $\dot{\epsilon}^+$ is driven by a thermal stress component *lower* than the applied stress, whereas $\dot{\epsilon}^-$ is driven by a local stress that is *enhanced* by the interaction of the recovering defects; this is an open task.

5. Summary

- In ufg Cu–Zr at $0.5 T_m$ recovery–strain ϵ^- connected with dynamic recovery of strain-induced crystal defects was found in tests with perturbation of the quasi-stationary (qs) state by load reductions. ϵ^- adds to the strain ϵ^+ connected with dislocation generation and storage.
- The stress dependence of $\dot{\epsilon}^+$ yields an activation volume consistent with the classical theory of thermally activated glide.
- The recovery–strain rate $\dot{\epsilon}^-$ contributes 10% to 30% to the quasi-stationary strain rate $\dot{\epsilon}_{qs}$. This fraction for ufg Cu–Zr with high volume fraction of HABs is similar to the one commonly reported for cg materials with high volume fraction of LABs. That could mean that boundaries play qualitatively similar roles in mediating dynamic recovery independent of their misorientation.
- The values of $\dot{\epsilon}_{cs}^-$ (at constant structure) and $\dot{\epsilon}_{qs}$ (at quasi-stationary structure) are relatively similar for large load reductions, even though the microstructures, in particular the dislocation structures, should differ significantly. This becomes understandable, if promotion of recovery by internal forward stresses is taken into account.
- Combining the rates of recovery–strain in the qs state and after perturbation of monotonic flow seems promising to better understand the mechanism of dynamic recovery of crystal defects, limiting the deformation strength under monotonic as well as cyclic loading conditions.

Author Contributions: Conceptualization, W.B. and P.K.; methodology, V.S., J.D., P.K. and P.E.; software, W.B. and P.E.; validation, P.K., J.D.; formal analysis, W.B.; investigation, V.S., J.D., P.K.; resources, J.D.; data curation, J.D., P.K. and W.B.; writing–original draft preparation, W.B.; writing–review and editing, W.B., P.K. and P.E.; visualization, W.B.; J.D., P.K., W.B. and P.E.; supervision, W.B. and V.S.

Conflicts of Interest: The authors declare no conflict of interest.

Abbreviations

The following abbreviations are used in this manuscript:

qs	quasi-stationary
ECAP	equal channel angular pressing
cg	coarse-grained
ufg	ultrafine-grained
LAB	low-angle boundary
HAB	high-angle boundary

Appendix A. Determination of Inelastic Strain

The load F corresponding to an engineering stress

$$\sigma_{eng} = F/S_0 \quad (A1)$$

was varied in steps. Figure A1a shows an example. Assuming volume constancy, the cross section varies with the gauge length

$$l = l_0 + \Delta l, \quad (\text{A2})$$

where Δl is the measured length change, as

$$S = S_0 l_0 / l = S_0 \exp(-\epsilon_{\text{tot}}), \quad \epsilon_{\text{tot}} = \ln(l/l_0) \quad (\text{A3})$$

where ϵ_{tot} is the total “true” strain. Figure A1b shows the variation of ϵ_{tot} with time t corresponding to Figure A1a. The ϵ_{tot} -steps in Figure A1b result from the changes of the elastic strain related with the changes of F . To eliminate these steps the elastic strain must be estimated. This was done in the following straightforward manner. The elastic strain is composed from two components:

$$\epsilon_{\text{el}} = \epsilon_{\text{el,Cu}} + \epsilon_{\text{mach}}. \quad (\text{A4})$$

$\epsilon_{\text{el,Cu}}$ is the elastic strain of the gauge length l of the specimen described by:

$$\epsilon_{\text{el,Cu}} = \sigma / E \quad (\text{A5})$$

with

$$\sigma = F_c / S \approx \sigma_{\text{eng}} \exp(\epsilon_{\text{tot}}) \quad (\text{A6})$$

as “true” stress acting in the gauge length and $E \approx 9 \times 10^4$ MPa as elastic tensile modulus (Young’s modulus) of Cu. ϵ_{mach} is the elastic strain

$$\epsilon_{\text{mach}} = \Delta l_{\text{mach}} / l \quad (\text{A7})$$

resulting from all parts of specimen and machine entering the measured length change outside the gauge length l . The unknown elastic machine length change was determined in an iterative manner so that the elastic steps in the $\epsilon_{\text{tot}}-t$ plots like Figure A1b were optimally suppressed.

An analytical formulation with a power law:

$$\Delta l_{\text{mach}} / \text{mm} \approx c_1 (F_c / \text{N})^{c_2} - c_3. \quad 0.001 < c_3 < 0.006 \quad (\text{A8})$$

with $c_1 = 2.23 \times 10^{-4}$, $c_2 = 0.74$ and a constant c_3 turned out to be comfortable and sufficiently exact. The approximate inelastic strain then follows as:

$$\epsilon_{\text{inel}} = \epsilon_{\text{tot}} - \epsilon_{\text{el}}. \quad (\text{A9})$$

Individual choice of c_3 for each test proved reasonable to compensate systematic errors of the Δl -signal near $F = 0$ before the motions of specimen and strain gages become uniaxial. In a final step the stress was corrected by changing Equation (A6) to

$$\sigma \approx F_c / S = \sigma_{\text{eng}} \exp(\epsilon_{\text{inel}}). \quad (\text{A10})$$

This has only marginal influence on the results. Figure A1c shows that the elastic steps from Figure A1b have virtually disappeared. Some gaps in the curves are caused by data acquisition problems. The test includes a small stress increase at $t \approx 300$ s followed by stepwise unloading within less than 30 s. It is seen how the (inelastic) strain ϵ_{inel} continues to increase till 307 s and then starts to decrease. This decrease is called anelastic, because it is reversible on a macroscopic level. The elimination of the elastic strain helps to visualize the anelastic response that is less pronounced than the elastic one (also in comparison to the elastic response of the specimen). Equation (A7) may cause an elastic overcorrection at stresses below 100 MPa. However, this is irrelevant for the inelastic

strain rates in the periods of relatively constant load, where the major elastic strain component resulting from Δl_{mach} remains constant.

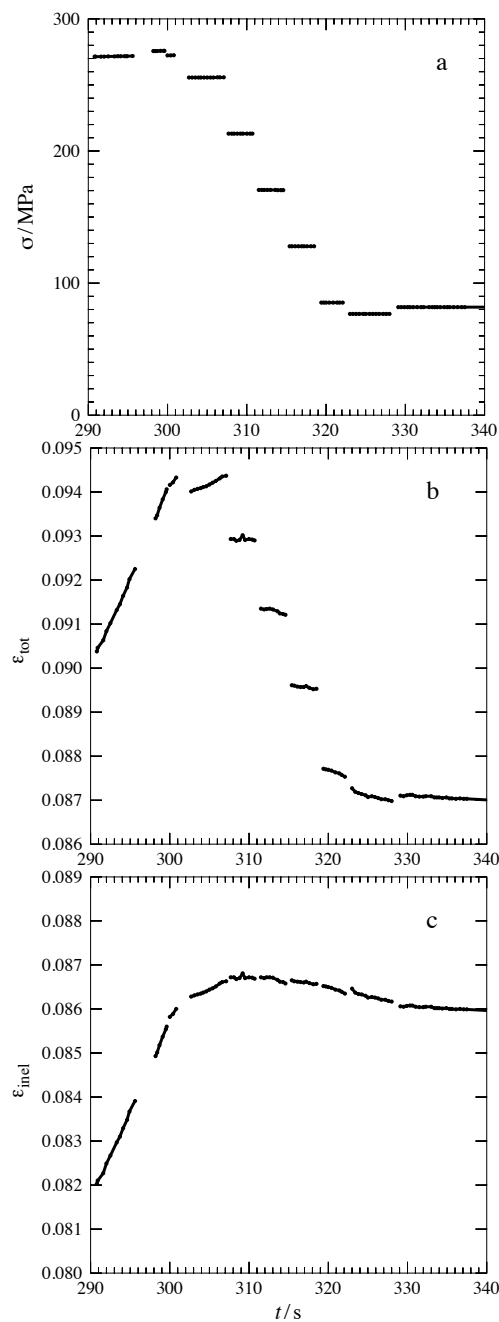


Figure A1. (a) Stress σ , (b) total strain ϵ_{tot} with elastic strains from machine and specimen, (c) inelastic strain ϵ_{inel} versus time t in load change test on 8Cu–Zr at 673 K.

Appendix B. Activation Volume of Dislocation Glide

Glide in the course of expansion of dislocation loops bounding the slipped areas causes an inelastic strain rate $\dot{\epsilon}^+$. It is driven by the resolved shear stress σ/M , where M is the geometrical factor of conversion from normal to shear stress and strain (for untextured face-centered polycrystals: Taylor

factor = 3.06), k_B is the Boltzmann constant, and is supported by thermally activated overcoming of thermal obstacles. The operational activation volume is defined by

$$V_{\text{op}}^+ = k_B T \frac{d \ln \dot{\epsilon}^+}{d\sigma/M} \quad (\text{A11})$$

To get a rough estimate of $V_{\text{gl}}^{\text{op}}$ we tentatively use the classical model of thermally activated glide through a field of point-like repulsive obstacles. According to this model the activation volume is

$$V^+ = b \lambda_{\text{gl}} \Delta x_{\text{gl}}. \quad (\text{A12})$$

where λ_{gl} and Δx_{gl} are obstacle spacing and width, respectively. Equation (A12) holds under the condition that the microstructure including the internal stresses remains constant in the change test. If

- λ_{gl} is set equal to the expected spacing of free dislocations, bG/σ , and
- Δx_{gl} is approximated by b ,

V^+ becomes a simple function of stress:

$$V^+ \approx b^3 G/\sigma. \quad (\text{A13})$$

By approximating V_{op}^+ in Equation (A11) by V^+ from Equation (A13) and using the mathematical identity $d\sigma = \sigma d \ln \sigma$ one arrives at a simple estimate

$$n_{\text{cs,est}}^+ \equiv \frac{b^3 G}{M k_B T}. \quad (\text{A14})$$

of the stress exponent of $\dot{\epsilon}^+$ at constant structure:

$$n_{\text{cs}}^+ = \frac{\partial \ln \dot{\epsilon}^+}{\partial \ln \sigma}. \quad (\text{A15})$$

(Meanwhile it has become customary to neglect the condition of constant structure; this leads to a mix-up with the qs rate sensitivity [16,38].) The estimate $n_{\text{cs,est}}^+$ is independent of σ and inversely proportional to temperature T for a given material.

citeyearref-journal-3b, p.475). This produces: Wong (1999, p. 328; 2000, p. 475)

References

1. Sherby, O.D.; Burke, P.M. Mechanical Behaviour of Crystalline Solids at Elevated Temperature. *Progr. Mater. Sci.* **1968**, *13*, 323–390, doi:10.1016/0079-6425(68)90024-8. [[CrossRef](#)]
2. Takeuchi, S.; Argon, A. Steady-state creep of alloys due to viscous motion of dislocations. *Acta Metall.* **1976**, *24*, 883–889, [[CrossRef](#)]
3. Čadež, J. *Creep in Metallic Materials*; Elsevier: Amsterdam, The Netherlands, 1988.
4. Blum, W.; Nix, W.D. Strain associated with recovery. *Res. Mech. Lett.* **1981**, *1*, 235–240.
5. Blum, W. On the Evolution of the Dislocation Structure during Work Hardening and Creep. *Scr. Metall.* **1984**, *18*, 1383–1388, doi:10.1016/0036-9748(84)90370-3. [[CrossRef](#)]
6. Mohamed, F.A.; Langdon, T.G. The transition from dislocation climb to viscous glide in creep of solid solution alloys. *Acta Metall.* **1974**, *22*, 779–788. [[CrossRef](#)]
7. Lindroos, V.; Mikk-oja, H. The structure and formation of dislocation networks in aluminium-magnesium alloys. *Phil. Mag.* **1967**, *16*, 593–610. [[CrossRef](#)]
8. Blum, W. Dislocation Models of Plastic Deformation of Metals at Elevated Temperatures. *Z. Metallkde.* **1977**, *68*, 484–492.
9. Caillard, D. In situ creep experiments in weak beam conditions, in Al at intermediate temperature, Interaction of dislocations with subboundaries. *Acta Metall.* **1984**, *32*, 1483–1491. [[CrossRef](#)]

10. Petegem, S.V.; Brandstetter, S.; Schmitt, B.; Swygenhoven, H.V. Creep in nanocrystalline Ni during X-ray diffraction. *Scr. Mater.* **2009**, *60*, 297–300, doi:10.1016/j.scriptamat.2008.10.034. [CrossRef]
11. Exell, S.F.; Warrington, D.H. Sub-grain Boundary Migration in Aluminum. *Philos. Mag. A* **1972**, *26*, 1121–1136. [CrossRef]
12. Gorkaya, T.; Molodov, D.A.; Gottstein, G. Stress-driven migration of symmetrical $\langle 100 \rangle$ tilt grain boundaries in Al bicrystals. *Acta Mater.* **2009**, *57*, 5396–5405. [CrossRef]
13. Humphreys, F.J.; Hatherly, M. *Recrystallization and Related Annealing Phenomena*; Elsevier Science: Oxford, UK, 1995.
14. Milička, K. Constant structure creep in metals after stress reduction in steady state stage. *Acta Metall. Mater.* **1993**, *41*, 1163–1172. [CrossRef]
15. Milička, K. Constant structure experiments in high temperature primary creep of some metallic materials. *Metall. Mater.* **1994**, *42*, 4189–4199. [CrossRef]
16. Milička, K. Constant structure creep experiments on aluminium. *Kov. Mater.* **2011**, *49*, 307–318. [CrossRef]
17. Nix, W.D.; Ilschner, B. Mechanisms Controlling Creep of Single Phase Metals and Alloys. In *Proceedings of the 5th International Conference, Aachen, Germany, 27–31 August 1979*; Haasen, P., Gerold, V., Kostorz, G., Eds.; Pergamon Press: Oxford, UK, 1980; pp. 1503–1530.
18. Weckert, E.; Blum, W. Transient Creep of an Al-5 at%Mg Solid Solution. In *Draft of paper in Proc. 7th Int. Conf. on the strength of Metals and Alloys (ICSMA7), Montreal, 12–16 August 1985*; McQueen, H.J., Bailon, J.P., Dickson, J.I., Jonas, J.J., Akben, M.G., Eds.; Pergamon Press: London, UK, 1985; pp. 773–778.
19. Blum, W.; Weckert, E. On the Interpretation of the ‘Internal Stress’ determined from Dip Tests during Creep of Al-5 at% Mg. *Mater. Sci. Eng.* **1987**, *23*, 145–158. [CrossRef]
20. Hausselt, J.; Blum, W. Dynamic recovery during and after steady state deformation of Al-11wt%Zn. *Acta Metall.* **1976**, *24*, 1027–1039. doi:10.1016/0001-6160(76)90133-4. [CrossRef]
21. Müller, W.; Biberger, M.; Blum, W. Subgrain Boundary Migration during Creep of LiF, III. Stress Reduction Experiments. *Philos. Mag. A* **1992**, *66*, 717–728. [CrossRef]
22. Sun, Z.; Van Petegem, S.; Cervellino, A.; Durst, K.; Blum, W.; Van Swygenhoven, H. Dynamic recovery in nanocrystalline Ni. *Acta Mater.* **2015**, *91*, 91–100. doi:10.1016/j.actamat.2015.03.033. [CrossRef]
23. Sun, Z.; Van Petegem, S.; Cervellino, A.; Blum, W.; Van Swygenhoven, H. Grain size and alloying effects on dynamic recovery in nanocrystalline metals. *Acta Mater.* **2016**, *119*, 104–114, doi:10.1016/j.actamat.2016.08.019. [CrossRef]
24. Hasegawa, T.; Yakou, T.; Kocks, U. Length changes and stress effects during recovery of deformed aluminum. *Acta Metall.* **1982**, *30*, 235–243. [CrossRef]
25. Hasegawa, T.; Yakou, T.; Kocks, U.F. Forward and Reverse Rearrangements of Dislocations in Tangled walls. *Mater. Sci. Eng.* **1986**, *81*, 189–199. [CrossRef]
26. Kapoor, R.; Li, Y.J.; Wang, J.T.; Blum, W. Creep transients during stress changes in ultrafine-grained copper. *Scr. Mater.* **2006**, *54*, 1803–1807. doi:10.1016/j.scriptamat.2006.01.032. [CrossRef]
27. Blum, W. A new way to visualize back strain and recovery strain after stress reductions. *ResearchGate* **2019**. doi:10.13140/RG.2.2.18688.69127/2. [CrossRef]
28. Dvořák, J.; Blum, W.; Král, P.; Sklenička, V. Quasi-stationary strength and strain softening of Cu–Zr after predeformation by ECAP. *Preprints* **2019**, 2019090073. [CrossRef]
29. Frost, H.J.; Ashby, M.F. *Deformation-Mechanism Maps*; Pergamon Press: Oxford, UK, 1982.
30. Eisenlohr, P. SmooMuDS: Flexible Smoothing of Multi-Valued Data Series. 2006. Available online: http://www.gmp.wv.uni-erlangen.de/SmooMuDS_engl.php (accessed on 25 November 2019). doi:10.13140/2.1.3636.2566. [CrossRef]
31. Kocks, U.; Mecking, H. Physics and phenomenology of strain hardening: the FCC case. *Progr. Mater. Sci.* **2003**, *48*, 171–273. doi:10.1016/S0079-6425(02)00003-8. [CrossRef]
32. Nes, E. Modelling work hardening and stress saturation in FCC metals. *Progr. Mater. Sci.* **1998**, *41*, 129–193. doi:10.1016/S0079-6425(97)00032-7. [CrossRef]
33. Vogler, S.; Blum, W. Micromechanical Modelling of Creep in Terms of the Composite Model. In *Creep and Fracture of Engineering Materials and Structures*; Wilshire, B., Evans, R., Eds.; The Institute of Metals: London, UK, 1990; pp. 65–79.
34. Dupraz, M.; Sun, Z.; Brandl, C.; Van Swygenhoven, H. Dislocation interactions at reduced strain rates in atomistic simulations of nanocrystalline Al. *Acta Mater.* **2018**, *144*, 68–79. [CrossRef]

35. Kassner, M.; Pérez-Prado, M.T. Five-Power-Law Creep in Single Phase Metals and Alloys. *Progr. Mater. Sci.* **2000**, *45*, 1–102.10.1016/S0079-6425(99)00006-7. [[CrossRef](#)]
36. Blum, W.; Rosen, A.; Cegielska, A.; Martin, J.L. Two mechanisms of dislocation motion during creep. *Acta Metall.* **1989**, *37*, 2439–2453. [[CrossRef](#)]
37. Mekala, S.; Eisenlohr, P.; Blum, W. Control of dynamic recovery and strength by subgrain boundaries—Insights from stress-change tests on CaF₂ single crystals. *Philos. Mag.* **2011**, *91*, 908–931.10.1080/14786435.2010.535324. [[CrossRef](#)]
38. Blum, W. Discussion: Activation volumes of plastic deformation of crystals. *Scr. Mater.* **2018**, *146*, 27–30.10.1016/j.scriptamat.2017.10.029. [[CrossRef](#)]



© 2019 by the authors. Licensee MDPI, Basel, Switzerland. This article is an open access article distributed under the terms and conditions of the Creative Commons Attribution (CC BY) license (<http://creativecommons.org/licenses/by/4.0/>).